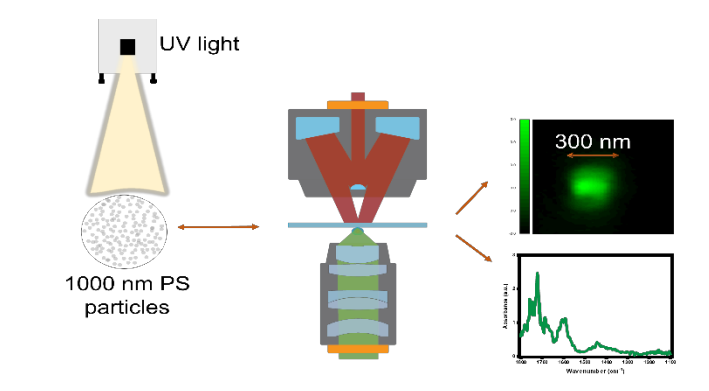
1	Single Particle Analysis of the Photodegradation of Submicron Polystyrene Particles using
2	Infrared Photothermal Heterodyne Imaging
3	
4	Authors: Ozioma Nwachukwu, a Kirill Kniazev, Angela Abarca Perez, Masaru Kuno, and
5	Kyle Doudrick <sup>a,*</sup>
6	
7	Affiliations:
8	<sup>a</sup> Department of Civil and Environmental Engineering and Earth Sciences, University of Notre
9	Dame, Notre Dame, IN 46556
10	<sup>b</sup> Department of Chemistry and Biochemistry, University of Notre Dame, Notre Dame, IN 46556
11	<sup>c</sup> Department of Physics and Astronomy, University of Notre Dame, Notre Dame, IN 46556
12	
13	*Corresponding Authors and Address:
14	Kyle Doudrick, Department of Civil and Environmental Engineering and Earth Sciences,
15	University of Notre Dame, Notre Dame, Indiana, USA, 46556
16	Phone: 5746310305
17	E-mail: kdoudrick@nd.edu
18	
19	
20	
21	Revision Date: 11/10/23

#### **ABSTRACT**

Sunlight is the predominant process for degrading plastics in the environment, but our current understanding of the degradation of smaller, submicron (<1000 nm) particles is limited due to prior analytical constraints. We used infrared photothermal heterodyne imaging (IR-PHI) to simultaneously analyze the chemical and morphological changes of single polystyrene (PS) particles (~1000 nm) when exposed to ultraviolet (UV) irradiation ( $\lambda$  = 250-400 nm). Within 6 hrs of irradiation, infrared bands associated with the backbone of PS decreased, accompanied by a reduction in the particle size. Concurrently, the formation of several spectral features due to photooxidation was attributed to ketones, carboxylic acids, aldehydes, esters, and lactones. Spectral outcomes were used to present an updated reaction scheme for the photodegradation of PS. After 36 hrs, the average particle size was reduced to 478  $\pm$  158 nm. The rate of size decrease and carbonyl band area increase were -24  $\pm$  3.0 nm hr<sup>-1</sup> and 2.1  $\pm$  0.6 cm<sup>-1</sup> hr<sup>-1</sup>, respectively. Use the size related rate, we estimated that under peak terrestrial sunlight conditions it will take less than 500 hrs for a 1000-nm PS particle to degrade to 1 nm.

- 36 Keywords: polystyrene, photodegradation, UV irradiation, IR spectroscopy, IR-PHI,
- 37 microplastics

# 39 TOC Art



## INTRODUCTION

Micro- and nanoplastics (MNPs) are emerging contaminants released from daily used goods such as textiles, 1 plastic packaging, 2,3 cosmetics, 4,5 and car tires. 6,7 MNPs primarily originate from the mechanical degradation of larger plastics from product use or exposure to environmental stressors such as water, wind, and sunlight irradiation. 8 MNPs have become ubiquitous in air, 9,10 soil, 11,12 surface waters, 13 municipal wastewater, 8,14,15 and drinking water. 16–18 Consequently, there is a growing concern regarding the potential environmental and health risks associated with MNPs. 8,19 While MNPs are not currently known to cause acute fatal effects on organisms, they are suspected to contribute to chronic toxicity, which is a significant concern in cases of long-term exposure. 8

Exposure of MNPs to ultraviolet (UV) irradiation is the primary pathway for their degradation in the ambient environment. <sup>20–25</sup> Photodegradation of plastics happens either through the direct breakdown of chromophoric groups via photolysis or indirectly through photooxidation in the presence of oxygen, involving chemical reactions initiated by light exposure. <sup>21</sup> Following photodegradation, the changes to the physical-chemical properties of the MNPs can influence their fate, transport, and toxicity in the environment. <sup>26</sup> To date, research on the photodegradation of plastics has mainly focused on larger macroplastics (>1 mm). <sup>27</sup> Smaller plastics are released during the degradation of macro-scale plastic products, <sup>44</sup> 47 but there is limited understanding of what happens to the released particles when exposed to sunlight. <sup>28</sup> <sup>31</sup>This is especially true for plastics less than 1000 nm due to the lack of suitable analytical tools capable of characterizing both chemical and morphological changes. Microscopic vibrational techniques like Raman and Fourier transform infrared spectroscopy (FTIR) are commonly used

for such analysis, but they are limited by spatial resolutions dictated by the optical diffraction limit. 32–38 Micro-FTIR has a lower spatial limit of approximately 5 μm, while Raman, although theoretically capable of a better resolution, is hindered by low scattering cross-sections. Here, we introduce the use of photothermal heterodyne imaging (IR-PHI) as a tool to analyze chemical and structural changes of submicron, or ultrafine, particles (<1000 nm) that occur during photodegradation. IR-PHI is a super-resolution infrared absorption technique with a current spatial resolution of 300 nm. 39–43 Through the process of deconvolution, it can effectively achieve a resolution of approximately 150 nm. 44

In this study, IR-PHI was used to investigate the photodegradation of single particle, submicron plastics exposed to UV irradiation ( $\lambda$  = 250-400 nm). This study provides the first proof-of-concept evidence for using IR-PHI to study the (photo)degradation mechanisms of submicron polymer particles. We selected polystyrene (PS) particles as a representative model submicron plastic due to their widespread use<sup>45,46</sup> and the potential toxicity concerns.<sup>24,47</sup> <sup>28–31</sup> We exposed PS particles (~1000 nm) to UV light and individually tracked and analyzed them after 0, 6, 18, and 36 hrs of irradiation. IR-PHI provided simultaneous information about the chemical and morphological changes of the particles. Two-dimensional correlation spectroscopy (2D-COS) was used to deconvolute IR bands and identify spectral features. The outcomes of the IR-PHI and 2D-COS analyses provided insights into the photodegradation mechanisms and enabled the development of an empirical kinetic model. Our results underscore the utility of IR-PHI as a tool to analyze MNPs at the single particle level, especially those less than 1000 nm, and the capability to elucidate specific degradation mechanisms.

#### MATERIALS AND METHODS

85

86

87

88

89

90

91

92

93

94

95

96

97

98

99

100

101

102

103

104

105

106

Sample Preparation. Spherical PS particles with a manufacturer reported average diameter of 1100 nm were used for all experiments (Sigma-Aldrich, MFCD00131491). The manufacturer reported that the composition of the stock solution is 30% PS, >69% water, 0.1-0.5% surfactants (Triton QS15 and Niaproof 4), and 0.2% inorganic salts (sodium bicarbonate and potassium sulfate). Both unwashed and washed samples were analyzed, and similar results were observed (see SI). All samples were prepared with ultrapure water (18.2 M $\Omega$ -cm) and loaded onto IR-grade calcium fluoride (CaF<sub>2</sub>) optical windows (25.0 mm in diameter and 0.5 mm in thickness, Crystran Ltd.). Before each experiment, the CaF<sub>2</sub> substrates were cleaned with acetone and ultrapure water and then cleaned using a Harrick PDC-32G Plasma Cleaner to make the substrate surface more hydrophilic. Oxygen plasma treatment of the substrate promotes hydroxylation of the surface by hydrogenating surface oxygen atoms, making it more hydrophilic so the liquid sample spreads evenly.<sup>48</sup> It is also important to promote even drying. The PS solution for the experiments was prepared by diluting the stock solution with ultrapure water to 1% V/V and then bath sonicated (Bransonic, M3800). Finally, 250 µL of the diluted PS solution was pipetted onto the CaF<sub>2</sub> substrates and left to dry in a fume hood for at least 12 hrs. No cross-contamination of the sample with MNPs from the surrounding environment during drying was observed on control samples.

**UV Irradiation.** After drying, the PS sample was exposed to UV irradiation using a 300 W short-arc Xe lamp (Newport 66483-300XF-R22 housing and power supply; 6258 lamp). The lamp housing was connected to a focusing lens assembly (Newport 77776) and a liquid light guide (LLG) with a transmission range of 300-650 nm (Newport 77556). This range provides

high-energy UV irradiation wavelengths emitted by the sun, and PS has a strong absorption at 318 nm. <sup>49</sup> Samples were placed approximately 5 mm from the LLG. The intensity spectrum was measured at the surface of the sample slide using a calibrated spectrometer (AvaSpec-EEEE-2-EVO) connected to a fiber optic (**Figure SI-1**). The light intensity and flux were 19224  $\mu$ W nm cm<sup>-2</sup> and  $2.59\times10^{17}$  photons s<sup>-1</sup> cm<sup>-2</sup>, respectively, as calculated from the integrated area of the spectrum. The flux was used to calculate the photon fluence (photons cm<sup>-2</sup>) at each time point of analysis (see SI for equations). Samples were irradiated in the dark for 36 hrs under ambient air conditions. During the irradiation, the sample was removed at t = 0, 6, 18, and 36 hrs for analysis by IR-PHI. Single particles were tracked using an etch mark made on the CaF<sub>2</sub> substrate. The temperature during irradiation was maintained at 23 ± 1 °C due to using the LLG, which removes infrared wavelengths.

IR-PHI Analysis. The absorption of the infrared light [M2 FireFly, tunable pulsed optical parametric oscillator (1040 to 1840 cm<sup>-1</sup>) 20 kHz] was probed using an LED 532 nm laser with a neutral density (ND) 1 filter. The PS sample was placed on a closed-loop piezo stage (MadCityLab Inc, MCLS03475) and moved within a 300  $\times$  300  $\mu$ m<sup>2</sup> area limit at the selected step velocity. Next, IR-PHI images were collected in a raster scanning fashion, where a diodepumped solid-state laser measured the sample's absorbance at a selected IR frequency (1500 cm<sup>-1</sup>). A large area (8 x 10  $\mu$ m<sup>2</sup>) containing particles of interest was first scanned at a step size of 0.2  $\mu$ m. Then, using the graphical user interface (GUI), the positions of particles of interest were identified and used to define the magnified scanning area (3 x 3  $\mu$ m<sup>2</sup>) at a step size of 0.05  $\mu$ m/pixel. Last, individual infrared absorption spectra are acquired by positioning pump and probe foci on individual particle positions and scanning incident pump wavelengths across the

optical parametric oscillator's tuning range. Each spectra data was normalized to the laser power to account for any intensity contributed by the laser and then divided by the peak intensity at 1600 cm<sup>-1</sup> as a reference<sup>51–53</sup> because it was not observed to change during irradiation. This enabled comparison between spectra obtained at various irradiation times for different particles. As a control, PS particles were analyzed for probe laser degradation by continuously exposing non-UV irradiated PS particles to the probe laser with an ND1 filter for 24 hrs. No spectra changes were observed with the ND1 filter; however, we did observe decreasing spectral features when an ND0.3 filter was used, so care should be taken with the choice of laser power and exposure time when analyzing polymers.

For particles, the IR-PHI intensity has a Gaussian profile across the particle width, where the corresponding full width at half maximum (FWHM) provides the approximate particle size. 40 To get the FWHM, the edge-to-edge profile of the raw images (intensity × pixel count) was first obtained using ImageJ. The pixel count was then converted to nanometers by multiplying the size in pixels by the image step size (e.g., 50 nm/pixel). Finally, using OriginPro, the resulting data were fitted with a Gaussian model and integrated to obtain the FWHM. This was repeated at 0, 45, and 90° profiles to get an average size for each particle. A resolution enhancement process was used on all IR-PHI images for visual representation purposes. Specifically, the 'interpolate.interp2d' function from the SciPy<sup>54</sup> Python library was used to double the image resolution.

**Two-dimensional correlation spectroscopy (2D-COS)**. Generalized 2D-COS was used to deconvolute the IR spectra to identify new spectral features and to examine sequential changes in the spectral bands. 2D-COS is a mathematical tool that interprets overlapping peaks of IR

spectra by spreading the peaks over a two-dimensional array.<sup>55</sup> 2D-COS analysis was completed in OriginPro using the built-in module. Synchronous and asynchronous plots were scaled using Pareto Scaling.

XPS Analysis. The surface chemistry of the PS before and after UV irradiation was characterized by X-Ray Photoelectron Spectroscopy (XPS; Kratos XSAM 800) at a pressure of 1.0 × 10<sup>-7</sup> Pa, with non-monochromatic Mg Kα radiation. Survey spectra were acquired with a pass energy of 100 eV and 25 eV for high-resolution spectra. The take-off angle for all experiments was 90°. Spectra peak was fitted using OriginPro analysis software with Linear and Shirley backgrounds. After subtracting the linear background, all spectra were fitted using 60% Gaussian/40% Lorentzian peaks, taking the minimum number of peaks consistent with the best fit. The binding energy scale was calibrated from C–C peaks at 284.8 eV. Carbon and oxygen peaks were fitted without the constraint of peak width.

AFM Analysis. An atomic force microscope (AFM; XE-70 Parc System) was used to obtain the size and morphology of single PS before and after UV irradiation. The AFM setup was mounted on a Herzan TS-150 vibration isolation table to ensure accurate imaging, effectively minimizing external vibrations during data acquisition. Non-contact mode imaging was performed using cantilevers with a natural resonant frequency of approximately 300 kHz. The scanning area for capturing AFM images was set to 4 × 4 μm, with a scan size of 256 × 256 pixels. The scanning rate, maintained at 0.5 Hz, was carefully chosen to prevent any movement of the spherical particles during imaging. In addition, image preprocessing for tilt correction was applied to compensate for the gradient background resulting from substrate tilt. AFM images were obtained at two time points: 0 and 18 hrs of UV irradiation. These images validated the

results obtained from IR-PHI, providing additional confirmation of the observed morphological changes.

## **RESULTS AND DISCUSSION**

IR-PHI analysis of the photodegradation of PS single particles. Figure 2 shows the IR-PHI analysis of three PS particles at t = 0 hrs (before irradiation). The IR-PHI spectra (Figure 1a) of the PS particles have major bands centered at 1444 cm<sup>-1</sup> [ $\delta$ (CH)+  $\nu$ (Semicircle Ring) + CH<sub>2</sub>], 1488 cm<sup>-1</sup> [ $\delta$ (CH)+  $\nu$ (Semicircle Ring)], and 1600 cm<sup>-1</sup> [ $\nu$ (Quadrant Ring)], which correspond with the characteristic bands of PS.<sup>56–59</sup> The region from 1650-1800 cm<sup>-1</sup> is associated with carbonyl groups (C=O), and its presence is likely due to either oxidation or minor contamination of the particle. The IR-PHI images (Figure 1b) confirmed the spherical shape of the PS particles, and the measured sizes for Particles 1, 2, and 3 were 1162, 1192, and 1198 nm (1184 ± 19 nm), respectively. These values closely correspond with the manufacturer's reported size of 1100 nm.

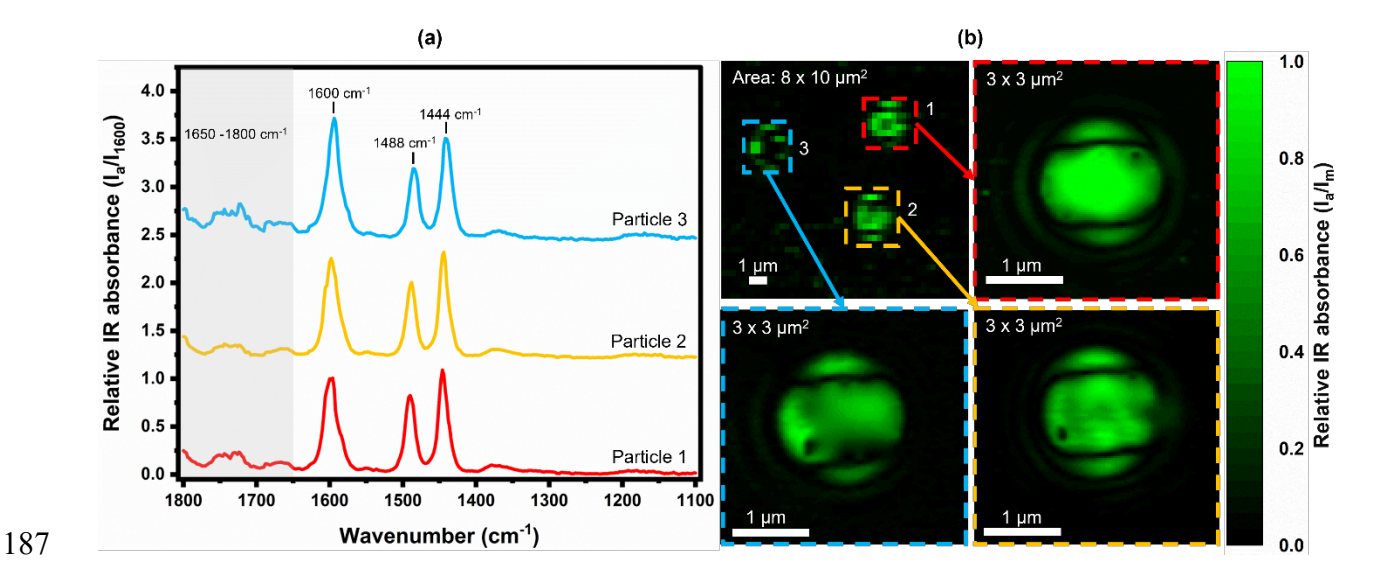


**Figure 1. (a)** IR-PHI spectra of Particles 1, 2, and 3 at 0 hrs and **(b)** IR-PHI images of Particles 1, 2, and 3 at 0 hrs. Images were taken at 1500 cm<sup>-1</sup>. The shaded gray area of the spectra in (a) represents the IR region between 1650 and 1800 cm<sup>-1</sup>.  $I_a$  is the absorbance intensity at a select frequency,  $I_{1600}$  is the absorbance intensity at 1600 cm<sup>-1</sup>, and  $I_m$  is the maximum absorbance intensity at the frequency used to image. The "basketball" lines and "ring" observed in the IP-PHI images are optical artifacts caused by scattered probe light diffraction.

The photodegradation of Particles 1, 2, and 3 was tracked for 36 hrs, and similar trends in changes in size and chemical composition were observed for all particles. Particle 2, referred to as the P2, was selected for discussion. **Figure 2** shows IR-PHI analysis of P2 after 6, 18, and 36 hrs of UV irradiation. Throughout the irradiation, the major bands centered at 1444 cm<sup>-1</sup> and 1488 cm<sup>-1</sup> were continually reduced, while several new bands formed between 1650 and 1800 cm<sup>-1</sup> (**Figure 2a**). This trend is due to the photodegradation of both CH and ring structures of PS and the formation of C=O groups. A major reduction in the intensity of the band centered at 1600 cm<sup>-1</sup> was not observed, though the band region widened, indicating the formation of new spectral features.

**Figure 2b** shows IR-PHI images of P2 after UV irradiation. After 6, 18, and 36 hrs, the average particle size decreased by approximately 29%, 35%, and 60% to  $844 \pm 58$ ,  $767 \pm 74$ , and  $478 \pm 158$  nm, respectively. Additionally, the morphology of the particle changed from spherical to oblong. The size and morphology reduction were confirmed with AFM (**Figure SI-2**). The size reduction and shape change indicated photodegradation occurred, presumably driven by polymer oxidation and chain scission, and this observation is synonymous with the disappearance of IR bands at  $1444 \text{ cm}^{-1}$  and  $1488 \text{ cm}^{-1}$ .

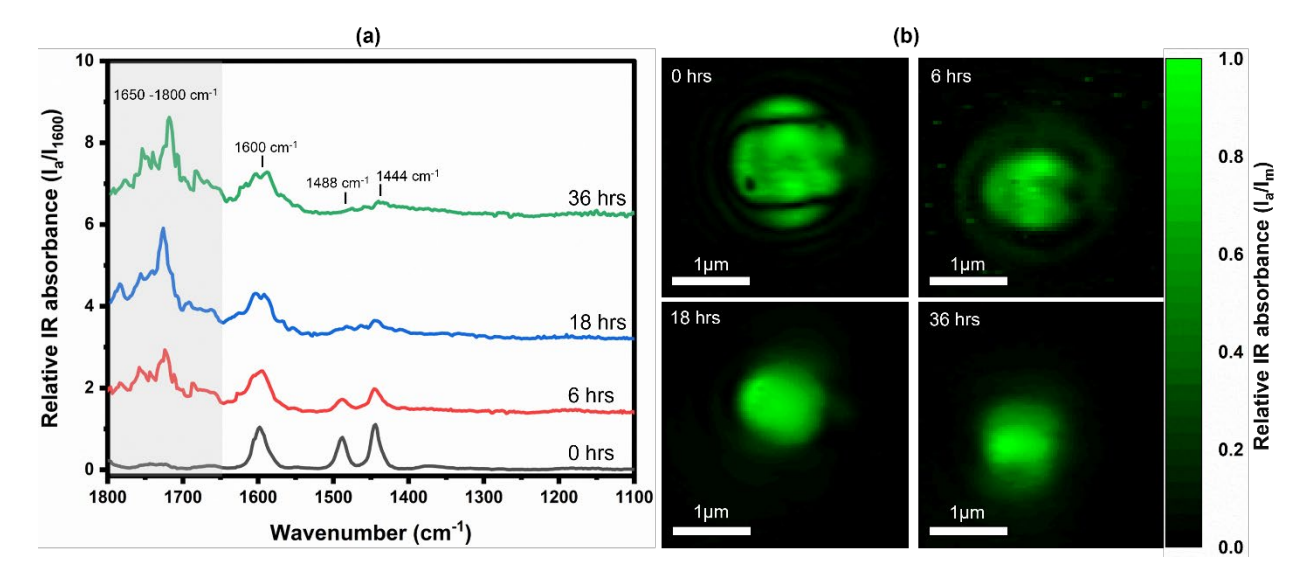


**Figure 2.** IR-PHI (a) spectra and (b) images of P2 after 0, 6, 18, and 36 hrs of UV irradiation. Images were taken at  $1500 \text{ cm}^{-1}$ . The shaded gray area of the spectra in (a) represents the IR region between 1650 and  $1800 \text{ cm}^{-1}$ .  $I_a$  is the absorbance intensity at a select frequency,  $I_{1600}$  is the absorbance intensity at  $1600 \text{ cm}^{-1}$ , and  $I_m$  is the maximum absorbance intensity at the frequency used to image. The "basketball" lines observed in the IP-PHI images at 0 hrs and the "ring" effect observed at 6 hrs are optical artifacts caused by scattered probe light diffraction.

Identification of Photodegradation Products and Mechanisms. XPS analysis of the C1s region for PS after UV irradiation for 0 and 36 hrs confirmed the formation of C=O groups (Figure 3). Before irradiation (Figure 3a), three peaks were present in the C1s, corresponding to

the C-C/C-H (285.6 eV) and C=C (284.7 eV). The  $\pi$ - $\pi$ \* shake-up satellite at 291.2 eV is from the C=C in the styrene rings. After 36 hrs of irradiation (**Figure 3b**), C=C reduced, C-C/C-H increased, and a new peak formed at 289 eV, assigned to C=O. These changes observed by XPS correlate to the IR-PHI spectra (**Figure 2**). The reduction of C=C suggests degradation and mass loss are occurring through a ring opening step that leads to radical formation, which reacts with photons, oxygen, and other groups in the PS structure to form low molecular weight products (e.g., carboxylic acids). Assuming the lower molecular weight products will further degrade and volatilize (e.g., carbon dioxide), C=C degradation supports the observed particle size reduction observed in the IR-PHI images (**Figure 2**).

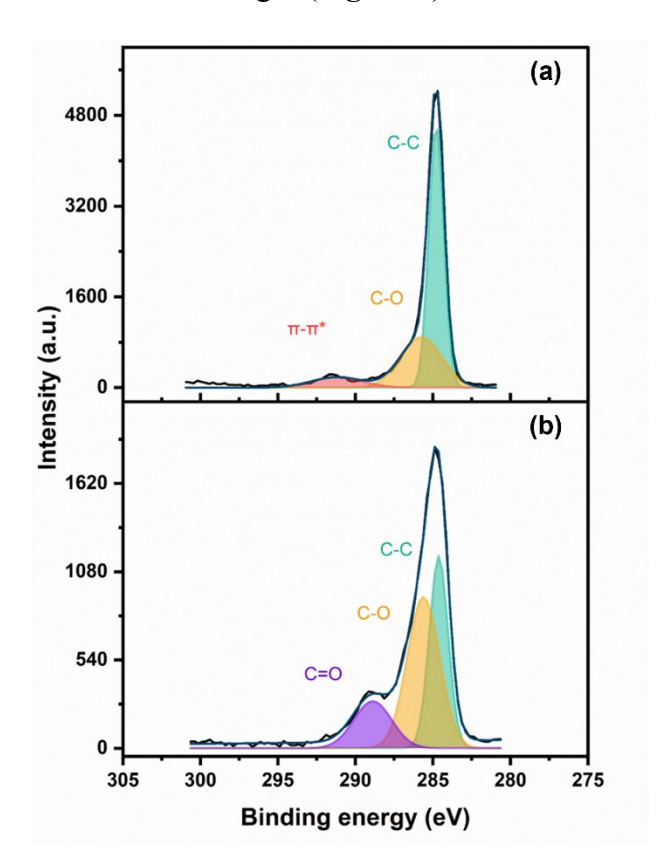


**Figure 3.** XPS analysis of PS after (a) 0 (b) 36 hrs of UV irradiation for the C1s region. The dotted line indicates the experimental data and the colored regions show the fitted peaks.

In the IR-PHI spectra (Figure 2), the bands centered at 1444 and 1488 cm<sup>-1</sup> are attributed to the semicircle vibrations of the styrene ring, whereas 1600 cm<sup>-1</sup> is attributed to the quadrant circle vibrations of the ring.<sup>27</sup> After 36 hrs of UV irradiation, 1444 and 1488 cm<sup>-1</sup> were reduced significantly, yet the intensity at 1600 cm<sup>-1</sup> remained mostly unchanged. The loss of the semicircle vibration in the ring suggests its frequency was coupled to the degradation of the backbone, whereas the stable quadrant ring vibration suggests that several byproducts still contained the styrene ring. Concurrently, these reactions led to the formation of several new bands in the carbonyl region between 1650 and 1800 cm<sup>-1</sup>, as illustrated in Figure 4a. Some of these bands have been identified in previous studies on the photodegradation of PS. <sup>20,25,45,49,51,56,58,62–79</sup> The 2D-COS asynchronous plot was used to deconvolute and identify C=O bands between 1650 and 1800 cm<sup>-1</sup> (Figure 4b). Several bands were identified, including 1654, 1665, 1674-1677, 1684, 1694, 1701, 1709, 1714-1717, 1720, 1728-1732, 1742-1744, 1751, 1757, 1760, 1770, 1774-1778, 1780, 1783-1786, 1791, and 1798 cm<sup>-1</sup>. **Table SI-1** summarizes the band positions and their possible assignments. The assignments broadly cover ketones, acids, quinones, aldehydes, esters, and lactones and include  $\alpha,\beta$ -unsaturated ketones, acetophenone, benzoic acid, muconic aldehyde, acetic, formic, and other small carboxylic acids.

234

235

236

237

238

239

240

241

242

243

244

245

246

247

248

249

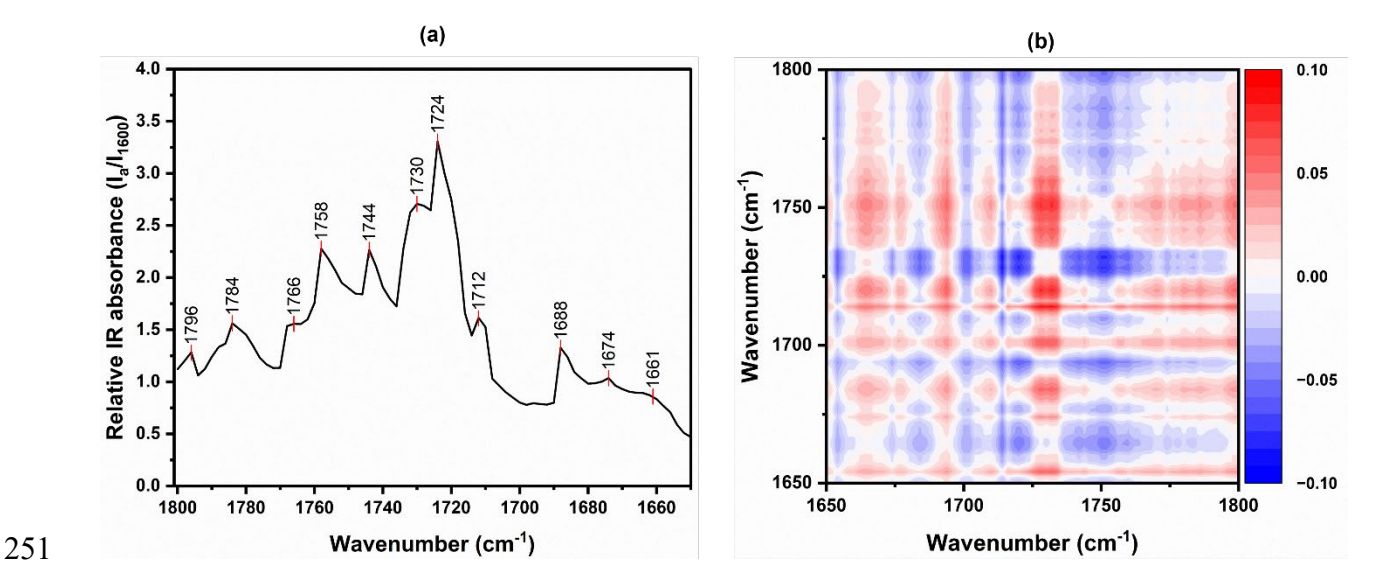


**Figure 4. (a)** IR-PHI spectra for the carbonyl region (1650-1800 cm<sup>-1</sup>) after 36 hrs of irradiation for P2.  $I_a$  is the absorbance intensity at a select frequency, and  $I_{1600}$  is the absorbance intensity at 1600 cm<sup>-1</sup>. **(b)** 2D-COS asynchronous plot for 1650-1800 cm<sup>-1</sup>.

The photooxidation reaction pathway of a polymer includes chain initiation, chain growth (propagation), radical chain branch formation, and chain termination. <sup>21,62</sup> In **Figure 5**, we propose an updated scheme for the photodegradation of PS, using outcomes of this study and building from the work of Gardette et al. <sup>80</sup> and Ranby et al. <sup>81</sup> Overall, the photodegradation of PS leads to the production of free radicals, scission of polymer chains, production of small molecules, and, ultimately, reduction of the polymer's molecular weight. <sup>25,45,80–83</sup> In the presence of oxygen (O<sub>2</sub>), photolysis of PS can be initiated through the styrene chromophore that absorbs UV photons (< 290 nm), <sup>62,84–87</sup> or via a charge transfer complex between oxygen and PS. <sup>62</sup> The excited species then reacts with PS to abstract an H and forms a PS alkyl radical (PS•; green color). Alternatively, the excited PS can react with O<sub>2</sub> to form singlet oxygen (<sup>1</sup>O<sub>2</sub>), which then reacts with PS to produce PS•. The PS• reacts with O<sub>2</sub> to form the PS peroxy radical (PS-OO•; red color). The peroxy radical then abstracts an H from an adjacent PS chain to form PS

hydroperoxide (PS-OOH) and another PS•, which will then react to form more PS-OOH. The PS-OOH directly photolyzes at 313 nm<sup>27,88</sup> to form the PS alkoxy radical (PS-O•, blue color) and a hydroxide radical (•OH). The concentration of PS-OOH eventually becomes the predominant absorber of incident radiation, and the photodegradation of PS-OOH becomes the predominant reaction.<sup>27</sup>

268

269

270

271

272

273

274

275

276

277

278

279

280

281

282

283

284

285

286

287

There are several possible pathways of degradation for PS-OO• and PS-O•. PS-OO• can be directly photolyzed to hydroxyphenyl anones and CH<sub>2</sub> or CH<sub>2</sub>CH<sub>3</sub> radicals, which is evident from the loss of IR peaks at 1450 cm<sup>-1</sup> and 1500 cm<sup>-1</sup>. It can also be photolyzed to form water and an alkoxy radical, which then abstracts an H from a neighboring PS to form PS• and 2phenylbut-3-en-2-ol. PS-O• can undergo scission at the α-carbon or react with PS.<sup>87</sup> The scission can occur at the C-CH<sub>2</sub> and form an end-chain acetophenone (1690 cm<sup>-1</sup>), which then either photolyzes to form acetophenone (1690 cm<sup>-1</sup>) or several products including benzaldehyde (1704 cm<sup>-1</sup>), benzoic acid (1698/1732 cm<sup>-1</sup>), benzoic anhydride (1725/1785 cm<sup>-1</sup>), and chain-end ketones (1725 cm<sup>-1</sup>). The latter can further photolyze to form chain-end acetic acid (1710/1753 cm<sup>-1</sup>) and acetic acid (1710 cm<sup>-1</sup>). These reactions would also result in the loss of CH groups. Acetophenone will photolyze to eventually form formic acid (1710 cm<sup>-1</sup>). The scission can also occur at the C-Ph and form a chain-ketone, which would undergo a Norrish reaction 89,90 to form PS• and benzene. If PS-O• reacts with PS, it will abstract an H to form PS• and phenyl alcohol, which will further react with photons, O<sub>2</sub>, •OH from the PS-OOH degradation to quinones (1665 cm<sup>-1</sup>), lactones (1780-1798 cm<sup>-1</sup>), and lower molecular weight byproducts.

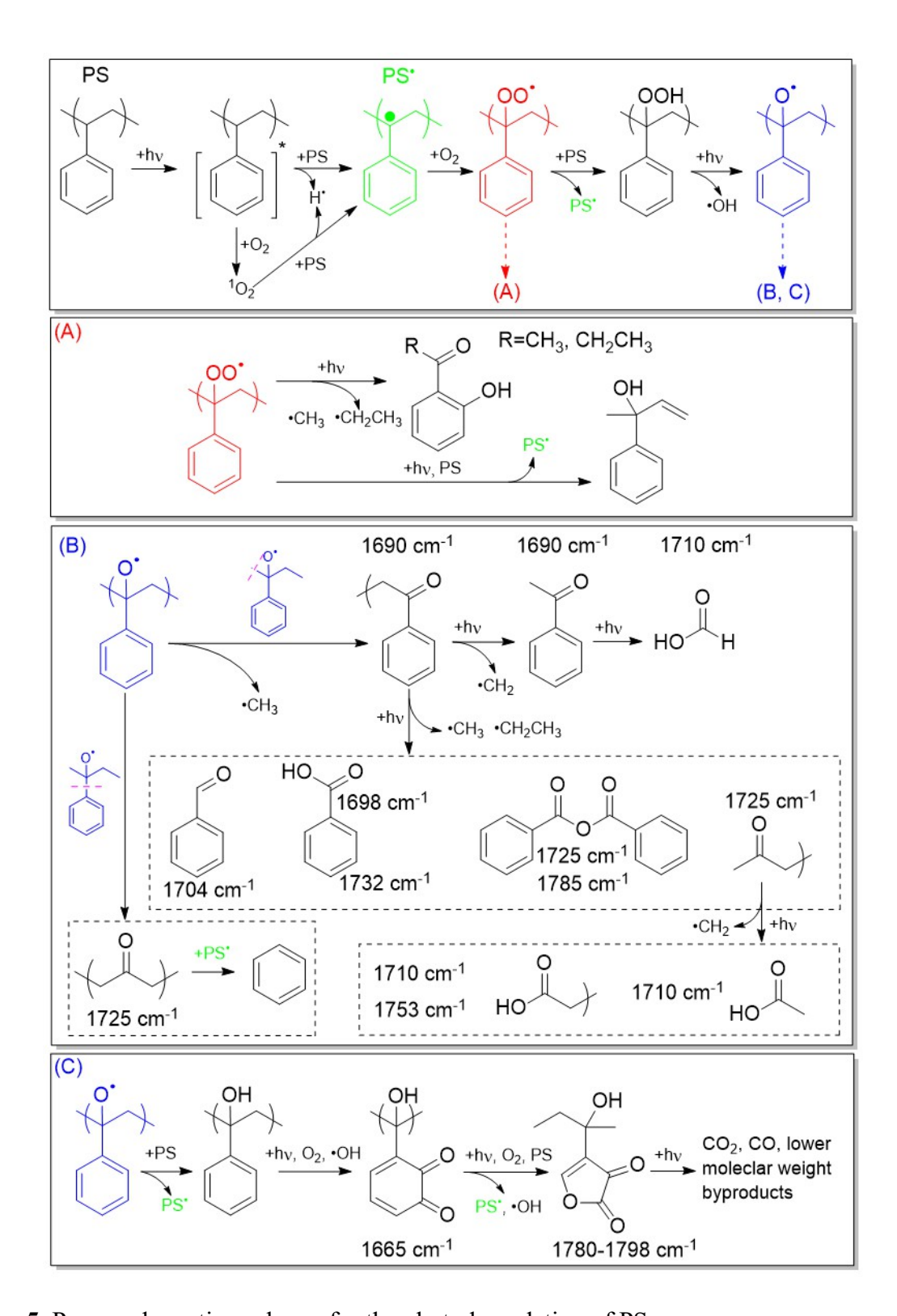


Figure 5. Proposed reaction scheme for the photodegradation of PS.

**Kinetics.** The depth of penetration for UV light through polymers tends to be much greater than the 1-µm size of the particles used in this study. 91-93 Thus, the photodegradation of the particles were presumably not strictly a surface phenomenon. The IR-PHI spectral results support this notion because peaks at 1444/1488 cm<sup>-1</sup> continued to disappear rather than stay steady, as would be expected as surface layers are degraded and bulk material is exposed. Regarding the kinetics of photodegradation, the formation of several byproducts simultaneously (i.e., Figure 4) makes it difficult to propose reaction pathways or determine specific rate laws. Hence, empirical kinetic models using the carbonyl region and particle size were more appropriate for identifying general trends. Figure 6 shows the average area of the carbonyl region (i.e., from 1650 to 1800 cm<sup>-1</sup>) and the average particle size for P1, P2, and P3 as a function of the irradiation time at 0, 6, 18, and 36 hrs. The time points correlate to photon fluences of 0, 5.60, 1.68, and 3.36 photons  $\times$  10<sup>21</sup> cm<sup>-2</sup>, respectively. The average carbonyl band area inversely correlated with the average particle size, confirming that the formation of byproducts containing C=O groups was ultimately responsible for the photodegradation of the PS and the corresponding decrease in size. A linear model was fitted to each dataset to obtain an approximate rate. The rate of size decrease and carbonyl band area increase was  $-24 \pm 3.0$  nm hr <sup>1</sup> and  $2.1 \pm 0.6$  cm<sup>-1</sup> hr<sup>-1</sup>, respectively. We can use the rate of size change to estimate the approximate time it would take to photodegrade the particle N\%. Assuming a peak sunlight intensity in the UV region of approximately 3000 µW cm<sup>-2</sup> (Solar Constant of 1380 W m<sup>-2</sup> / 1.38 atmospheric correction × 3% UV), the UV intensity of this study was roughly 6.4 times greater than peak sunlight. If all the UV photons of terrestrial sunlight participated equally in the photodegradation of a 1000 nm PS particle (i.e., a photon at 250 nm is the same as one at 400

290

291

292

293

294

295

296

297

298

299

300

301

302

303

304

305

306

307

308

309

310

nm), then the time required to reduce the particle to 1 nm at peak irradiation (noontime, summer) would be ~265 hrs. Thus, while microplastics are expected to be long lived in the environment, this calculation suggests that submicron plastic particles will have a comparatively short lifetime.

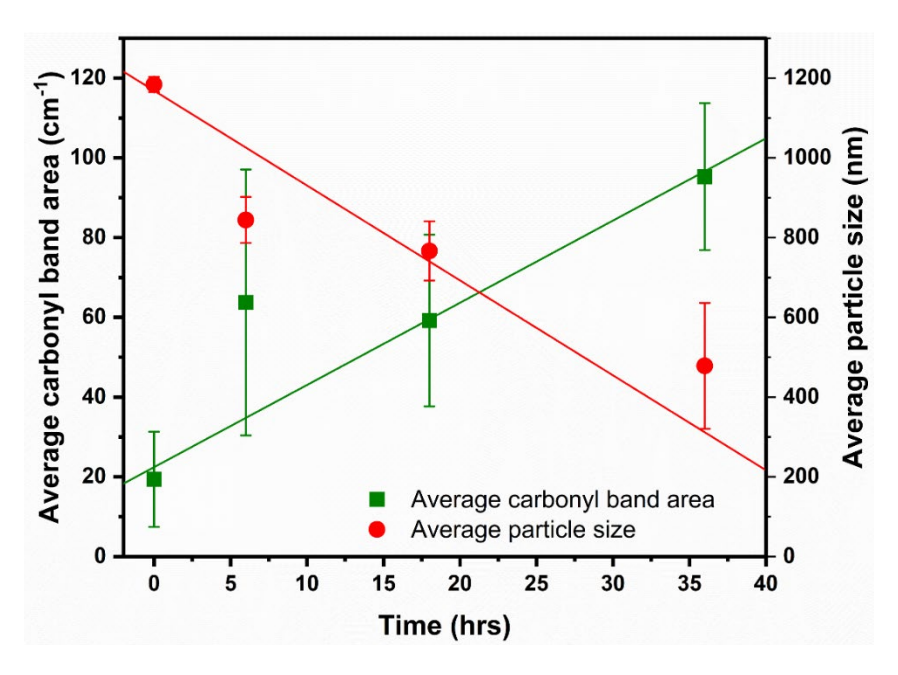


**Figure 6.** Average area of the carbonyl band (left axis) and average particle size (right axis) as a function of time for P1, P2, and P3. The data was fitted with a linear function, with  $R^2 = 0.94$  and 0.84 for the carbonyl area and particle size, respectively. The carbonyl band area was relative to  $1600 \text{ cm}^{-1}$  (i.e.,  $I_a/I_{1600}$ ).

## **SUPPORTING INFORMATION**

321 The supporting information is available free of charge at XXXX.

Detailed photon fluence calculation, lamp intensity spectrum, AFM characterization result, additional IR-PHI figures, washed PS IR-PHI spectra, and washed PS kinetics plot.

## **ACKNOWLEDGMENT**

The authors thank Evgenii Zaitsev for programming and designing the graphical user interface (GUI) for the IR-PHI instrument. We thank the ND Energy Materials Characterization Facility (MCF) for the use of the Harrick PDC-32G Plasma Cleaner. The MCF is funded by the Sustainable Energy Initiative (SEI), which is part of the Center for Sustainable Energy at Notre Dame (ND Energy). Masaru Kuno thanks the NSF under award CHE1954724 for financial support.

## 332 **REFERENCES**

- 333 (1) Yang, T.; Luo, J.; Nowack, B. Characterization of Nanoplastics, Fibrils, and Microplastics
- Released during Washing and Abrasion of Polyester Textiles. *Environ Sci Technol* **2021**,
- https://doi.org/10.1021/ACS.EST.1C04826/ASSET/IMAGES/LARGE/ES1C04826\_0005.
- JPEG.
- 338 (2) Jadhav, E. B.; Sankhla, M. S.; Bhat, R. A.; Bhagat, D. S. Microplastics from Food
- Packaging: An Overview of Human Consumption, Health Threats, and Alternative
- 340 Solutions. Environ Nanotechnol Monit Manag 2021, 16, 100608.
- 341 https://doi.org/10.1016/J.ENMM.2021.100608.
- 342 (3) Claudia, C.; la Spina, R.; Mehn, D.; Fumagalli, F.; Ceccone, G.; Valsesia, A.; Gilliland, D.
- Detecting Micro-and Nanoplastics Released from Food Packaging: Challenges and
- 344 Analytical Strategies. *Polymers (Basel)* **2022**, 14 (6).
- 345 https://doi.org/10.3390/polym14061238.
- 346 (4) Hernandez, L. M.; Yousefi, N.; Tufenkji, N. Are There Nanoplastics in Your Personal
- Care Products? Environ Sci Technol Lett 2017, 4 (7), 280–285.
- 348 https://doi.org/10.1021/ACS.ESTLETT.7B00187/ASSET/IMAGES/LARGE/EZ-2017-
- 349 00187H 0003.JPEG.
- 350 (5) Bashir, S. M.; Kimiko, S.; Mak, C. W.; Fang, J. K. H.; Gonçalves, D. Personal Care and
- 351 Cosmetic Products as a Potential Source of Environmental Contamination by

- Microplastics in a Densely Populated Asian City. Front Mar Sci 2021, 8, 604.
- 353 https://doi.org/10.3389/FMARS.2021.683482/XML/NLM.
- Tamis, J. E.; Koelmans, A. A.; Dröge, R.; Kaag, N. H. B. M.; Keur, M. C.; Tromp, P. C.;
- Jongbloed, R. H. Environmental Risks of Car Tire Microplastic Particles and Other Road
- Runoff Pollutants. *Microplastics and Nanoplastics 2021 1:1* **2021**, *1* (1), 1–17.
- 357 https://doi.org/10.1186/S43591-021-00008-W.
- 358 (7) Jan Kole, P.; Löhr, A. J.; van Belleghem, F. G. A. J.; Ragas, A. M. J. Wear and Tear of
- Tyres: A Stealthy Source of Microplastics in the Environment. *Int J Environ Res Public*
- 360 *Health* **2017**, *14* (10). https://doi.org/10.3390/IJERPH14101265.
- 361 (8) Sun, J.; Dai, X.; Wang, Q.; van Loosdrecht, M. C. M.; Ni, B. J. Microplastics in
- Wastewater Treatment Plants: Detection, Occurrence and Removal. *Water Res* **2019**, *152*,
- 363 21–37. https://doi.org/10.1016/J.WATRES.2018.12.050.
- 364 (9) Xie, Y.; Li, Y.; Feng, Y.; Cheng, W.; Wang, Y. Inhalable Microplastics Prevails in Air:
- Exploring the Size Detection Limit. Environ Int 2022, 162, 107151.
- 366 https://doi.org/10.1016/J.ENVINT.2022.107151.
- 367 (10) Yao, Y.; Glamoclija, M.; Murphy, A.; Gao, Y. Characterization of Microplastics in Indoor
- and Ambient Air in Northern New Jersey. Environ Res 2022, 207, 112142.
- 369 https://doi.org/10.1016/J.ENVRES.2021.112142.

- 370 (11) Wang, F.; Wang, Q.; Adams, C. A.; Sun, Y.; Zhang, S. Effects of Microplastics on Soil
- Properties: Current Knowledge and Future Perspectives. J Hazard Mater 2022, 424,
- 372 127531. https://doi.org/10.1016/J.JHAZMAT.2021.127531.
- 373 (12) Ding, L.; Huang, D.; Ouyang, Z.; Guo, X. The Effects of Microplastics on Soil
- Ecosystem: A Review. Curr Opin Environ Sci Health 2022, 26, 100344.
- 375 https://doi.org/10.1016/J.COESH.2022.100344.
- 376 (13) Zhang, S.; Zhang, W.; Ju, M.; Qu, L.; Chu, X.; Huo, C.; Wang, J. Distribution
- 377 Characteristics of Microplastics in Surface and Subsurface Antarctic Seawater. *Science of*
- 378 The Total Environment **2022**, 838, 156051.
- 379 https://doi.org/10.1016/J.SCITOTENV.2022.156051.
- 380 (14) Cheng, Y.; Lu, J.; Fu, S.; Wang, S.; Senehi, N.; Yuan, Q. Enhanced Propagation of
- 381 Intracellular and Extracellular Antibiotic Resistance Genes in Municipal Wastewater by
- Microplastics. Environmental Pollution 2022, 292, 118284.
- 383 https://doi.org/10.1016/J.ENVPOL.2021.118284.
- 384 (15) Priya, A.; Anusha, G.; Thanigaivel, S.; Karthick, A.; Mohanavel, V.; Velmurugan, P.;
- Balasubramanian, B.; Ravichandran, M.; Kamyab, H.; Kirpichnikova, I. M.; Chelliapan,
- 386 S. Removing Microplastics from Wastewater Using Leading-Edge Treatment
- Technologies: A Solution to Microplastic Pollution—a Review. *Bioprocess Biosyst Eng*
- 388 **2022**, *I*, 1–13. https://doi.org/10.1007/S00449-022-02715-X/FIGURES/9.

- 3896) Singh, S.; Trushna, T.; Kalyanasundaram, M.; Tamhankar, A. J.; Diwan, V. Microplastics in
- 390 Drinking Water: A Macro Issue. Water Supply 2022, 22 (5), 5650-5674.
- 391 https://doi.org/10.2166/WS.2022.189.
- 392 (17) Oni, B. A.; Sanni, S. E. Occurrence of Microplastics in Borehole Drinking Water and
- 393 Sediments in Lagos, Nigeria. Environ Toxicol Chem 2022, 00, 0-1.
- 394 https://doi.org/10.1002/ETC.5350.
- 393) Coffin, S.; Bouwmeester, H.; Brander, S.; Damdimopoulou, P.; Gouin, T.; Hermabessiere, L.;
- Khan, E.; Koelmans, A. A.; Lemieux, C. L.; Teerds, K.; Wagner, M.; Weisberg, S. B.; Wright, S.
- 397 Development and Application of a Health-Based Framework for Informing Regulatory Action in
- 398 Relation to Exposure of Microplastic Particles in California Drinking Water. *Microplastics and*
- 399 Nanoplastics 2022 2:1 **2022**, 2 (1), 1–30. https://doi.org/10.1186/S43591-022-00030-6.
- 400 (19) Su, Y.; Hu, X.; Tang, H.; Lu, K.; Li, H.; Liu, S.; Xing, B.; Ji, R. Steam Disinfection
- 401 Releases Micro(Nano)Plastics from Silicone-Rubber Baby Teats as Examined by Optical
- 402 Photothermal Infrared Microspectroscopy. Nat Nanotechnol 2022, 17 (1), 76–85.
- 403 https://doi.org/10.1038/S41565-021-00998-X.
- 4(24) Ghaffar, A.; Scott, A.; Scott, G. The Chemical and Physical Changes Occurring during U.V.
- 405 Degradation of High Impact Polystyrene. Eur Polym J 1975, 11 (3), 271–275.
- 406 https://doi.org/10.1016/0014-3057(75)90075-0.

- 4021) Sun, Y.; Yuan, J.; Zhou, T.; Zhao, Y.; Yu, F.; Ma, J. Laboratory Simulation of Microplastics
- 408 Weathering and Its Adsorption Behaviors in an Aqueous Environment: A Systematic Review \*.
- 409 **2020**. https://doi.org/10.1016/j.envpol.2020.114864.
- 410 (22) Feldman, D. Polymer Weathering: Photo-Oxidation. *J Polym Environ* **2002**, *10* (4).
- 4(2B) Gewert, B.; Plassmann, M. M.; Macleod, M. Pathways for Degradation of Plastic Polymers
- 412 Floating in the Marine Environment. Environ Sci Process Impacts 2015, 17 (9), 1513–1521.
- 413 https://doi.org/10.1039/C5EM00207A.
- 414 (24) Cai, L.; Wang, J.; Peng, J.; Wu, Z.; Tan, X. Observation of the Degradation of Three
- Types of Plastic Pellets Exposed to UV Irradiation in Three Different Environments.
- **2018**, *628–629*, 740–747. https://doi.org/10.1016/J.SCITOTENV.2018.02.079.
- 417 (25) Sikandar Shah, S.; Ahmad, I.; Ishaq, M. Degradation Study of Used Polystyrene with UV
- 418 Irradiation Valorization of Spent Lubricating Oil View Project Pyrolysis of Pololefins
- View Project Degradation Study of Used Polystyrene with UV Irradiation. Adv Mater Sci
- 420 **2017**, 2 (3), 1–6. https://doi.org/10.15761/AMS.1000130.
- 421 (26) Rai, P. K.; Sonne, C.; Brown, R. J. C.; Younis, S. A.; Kim, K. H. Adsorption of
- Environmental Contaminants on Micro- and Nano-Scale Plastic Polymers and the
- Influence of Weathering Processes on Their Adsorptive Attributes. *J Hazard Mater* **2022**,
- 424 427. https://doi.org/10.1016/J.JHAZMAT.2021.127903.

- 425 (27) Rabek, J. F. *Polymer Photodegradation*; Springer Berlin Heidelberg: Berlin, Heidelberg,
- 426 1995. https://doi.org/https://doi.org/10.1007/978-94-011-1274-1.
- 427 (28) Lambert, S.; Wagner, M. Characterisation of Nanoplastics during the Degradation of
- 428 Polystyrene. *Chemosphere* **2016**, *145*, 265.
- 429 https://doi.org/10.1016/J.CHEMOSPHERE.2015.11.078.
- 430 (29) Chen, H.; Xu, L.; Yu, K.; Wei, F.; Zhang, M. Release of Microplastics from Disposable
- Cups in Daily Use. Science of The Total Environment 2023, 854, 158606.
- 432 https://doi.org/10.1016/J.SCITOTENV.2022.158606.
- 433 (30) Lehner, R.; Weder, C.; Petri-Fink, A.; Rothen-Rutishauser, B. Emergence of Nanoplastic
- in the Environment and Possible Impact on Human Health. Environ Sci Technol 2019.
- https://doi.org/10.1021/ACS.EST.8B05512/ASSET/IMAGES/MEDIUM/ES-2018-
- 436 055122 0006.GIF.
- 437 (31) Zhang, K.; Su, J.; Xiong, X.; Wu, X.; Wu, C.; Liu, J. Microplastic Pollution of Lakeshore
- 438 Sediments from Remote Lakes in Tibet Plateau, China. *Environmental Pollution* **2016**,
- 439 219, 450–455. https://doi.org/10.1016/J.ENVPOL.2016.05.048.
- 4302) Mintenig, S. M.; Int-Veen, I.; Löder, M. G. J.; Primpke, S.; Gerdts, G. Identification of
- 441 Microplastic in Effluents of Waste Water Treatment Plants Using Focal Plane Array-Based
- 442 Micro-Fourier-Transform Infrared Imaging. Water Res 2017, 108, 365–372.
- 443 https://doi.org/10.1016/J.WATRES.2016.11.015.

- 444 (33) Tagg, A. S.; Sapp, M.; Harrison, J. P.; Sinclair, C. J.; Bradley, E.; Ju-Nam, Y.; Ojeda, J. J.
- 445 Microplastic Monitoring at Different Stages in a Wastewater Treatment Plant Using
- Reflectance Micro-FTIR Imaging. Front Environ Sci 2020, 8, 560949.
- 447 https://doi.org/10.3389/FENVS.2020.00145/BIBTEX.
- 448 (34) Tagg, A. S.; Sapp, M.; Harrison, J. P.; Ojeda, J. J. Identification and Quantification of
- 449 Microplastics in Wastewater Using Focal Plane Array-Based Reflectance Micro-FT-IR
- 450 Imaging. Anal Chem **2015**, 87 (12), 6032–6040.
- 451 https://doi.org/10.1021/ACS.ANALCHEM.5B00495/SUPPL FILE/AC5B00495 SI 001.
- 452 PDF.
- 453 (35) Lenz, R.; Enders, K.; Stedmon, C. A.; MacKenzie, D. M. A.; Nielsen, T. G. A Critical
- 454 Assessment of Visual Identification of Marine Microplastic Using Raman Spectroscopy
- for Analysis Improvement. Mar Pollut Bull 2015, 100 (1), 82–91.
- 456 https://doi.org/10.1016/J.MARPOLBUL.2015.09.026.
- 457 (36) Schymanski, D.; Goldbeck, C.; Humpf, H. U.; Fürst, P. Analysis of Microplastics in
- Water by Micro-Raman Spectroscopy: Release of Plastic Particles from Different
- 459 Packaging into Mineral Water. Water Res 2018, 129, 154–162.
- 460 https://doi.org/10.1016/J.WATRES.2017.11.011.
- 461 (37) Käppler, A.; Fischer, D.; Oberbeckmann, S.; Schernewski, G.; Labrenz, M.; Eichhorn, K.
- J.; Voit, B. Analysis of Environmental Microplastics by Vibrational Microspectroscopy:

- 463 FTIR, Raman or Both? Anal Bioanal Chem 2016, 408 (29), 8377-8391.
- 464 https://doi.org/10.1007/S00216-016-9956-3.
- 468) Vianello, A.; Boldrin, A.; Guerriero, P.; Moschino, V.; Rella, R.; Sturaro, A.; Da Ros, L.
- 466 Microplastic Particles in Sediments of Lagoon of Venice, Italy: First Observations on
- Occurrence, Spatial Patterns and Identification. Estuar Coast Shelf Sci 2013, 130, 54-61.
- 468 https://doi.org/10.1016/J.ECSS.2013.03.022.
- 469 (39) Pavlovetc, I. M.; Podshivaylov, E. A.; Chatterjee, R.; Hartland, G. V.; Frantsuzov, P. A.;
- Kuno, M. Infrared Photothermal Heterodyne Imaging: Contrast Mechanism and Detection
- 471 Limits. J Appl Phys **2020**, 127 (16), 165101.
- 472 https://doi.org/10.1063/1.5142277/15245037/165101 1 ACCEPTED MANUSCRIPT.P
- 473 DF.
- 474 (40) Kniazev, K.; Pavlovetc, I. M.; Zhang, S.; Kim, J.; Stevenson, R. L.; Doudrick, K.; Kuno,
- 475 M. Using Infrared Photothermal Heterodyne Imaging to Characterize Micro-and
- Nanoplastics in Complex Environmental Matrices. *Environ. Sci. Technol* **2021**, *55*, 30.
- 477 https://doi.org/10.1021/acs.est.1c05181.
- 478 (41) Pavlovetc, I. M.; Aleshire, K.; Hartland, G. V.; Kuno, M. Approaches to Mid-Infrared,
- Super-Resolution Imaging and Spectroscopy. *Physical Chemistry Chemical Physics* **2020**,
- 480 22 (8), 4313–4325. https://doi.org/10.1039/C9CP05815J.

- 481 (42) Bai, Y.; Yin, J.; Cheng, J. X. Bond-Selective Imaging by Optically Sensing the Mid-
- 482 Infrared Photothermal Effect. Sci Adv 2021, 7 (20).
- 483 https://doi.org/10.1126/SCIADV.ABG1559.
- 484) Li, Z.; Aleshire, K.; Kuno, M.; Hartland, G. V. Super-Resolution Far-Field Infrared Imaging by
- 485 Photothermal Heterodyne Imaging. *Journal of Physical Chemistry B* **2017**, *121* (37), 8838–8846.
- 486 https://doi.org/10.1021/ACS.JPCB.7B06065/ASSET/IMAGES/LARGE/JP-2017-
- 487 06065K 0003.JPEG.
- 488 (44) Zhang, S.; Kniazev, K.; Pavlovetc, I. M.; Zhang, S.; Stevenson, R. L.; Kuno, M. Deep
- Image Restoration for Infrared Photothermal Heterodyne Imaging. Journal of Chemical
- 490 *Physics* **2021**, 155 (21).
- 491 https://doi.org/10.1063/5.0071944/14879565/214202\_1\_ACCEPTED\_MANUSCRIPT.P
- 492 DF.
- 493 (45) Yousif, E.; Haddad, R. Photodegradation and Photostabilization of Polymers, Especially
- 494 Polystyrene: Review. *Springerplus* **2013**, *2* (1). https://doi.org/10.1186/2193-1801-2-398.
- 495 (46) Halden, R. U. Plastics and Health Risks.
- 496 http://dx.doi.org/10.1146/annurev.publhealth.012809.103714 **2010**, 31, 179–194.
- 497 https://doi.org/10.1146/ANNUREV.PUBLHEALTH.012809.103714.
- 498 (47) Oslakovic, C.; Cedervall, T.; Linse, S.; Dahlbäck, B. Polystyrene Nanoparticles Affecting
- 499 Blood Coagulation. *Nanomedicine* **2012**, 8 (6), 981–986.
- 500 https://doi.org/10.1016/J.NANO.2011.12.001.

- 501 (48) Li, D.; Xiong, M.; Wang, S.; Chen, X.; Wang, S.; Zeng, Q. Effects of Low-Temperature
- Plasma Treatment on Wettability of Glass Surface: Molecular Dynamic Simulation and
- 503 Experimental Study. Appl Surf Sci 2020, 503, 144257.
- 504 https://doi.org/10.1016/J.APSUSC.2019.144257.
- 505 (49) Dong, S.; Yan, X.; Yue, Y.; Li, W.; Luo, W.; Wang, Y.; Sun, J.; Li, Y.; Liu, M.; Fan, M.
- H2O2 Concentration Influenced the Photoaging Mechanism and Kinetics of Polystyrene
- Microplastic under UV Irradiation: Direct and Indirect Photolysis. J Clean Prod 2022,
- 508 380, 135046. https://doi.org/10.1016/J.JCLEPRO.2022.135046.
- 509 (50) Pavlovetc, I. M.; Podshivaylov, E. A.; Frantsuzov, P. A.; Hartland, G. v.; Kuno, M. K.
- Ouantitative Infrared Photothermal Microscopy. 2020, 41.
- 511 https://doi.org/10.1117/12.2545159.
- 512 (51) Castro Monsores, K. G. de; Silva, A. O. da; Sant' Ana Oliveira, S. de; Weber, R. P.; Filho,
- P. F.; Monteiro, S. N. Influence of Ultraviolet Radiation on Polystyrene. *Journal of*
- Materials Research and Technology 2021, 13, 359–365.
- 515 https://doi.org/10.1016/J.JMRT.2021.04.035.
- 516 (52) Ojeda, T.; Freitas, A.; Birck, K.; Dalmolin, E.; Jacques, R.; Bento, F.; Camargo, F.
- Degradability of Linear Polyolefins under Natural Weathering. *Polym Degrad Stab* **2011**,
- 518 96 (4), 703–707. https://doi.org/10.1016/J.POLYMDEGRADSTAB.2010.12.004.
- 519 (53) Chiellini, E.; Corti, A.; D'Antone, S.; Baciu, R. Oxo-Biodegradable Carbon Backbone
- Polymers Oxidative Degradation of Polyethylene under Accelerated Test Conditions.

- 521 Polym Degrad Stab 2006, 91 (11), 2739–2747.
   522 https://doi.org/10.1016/J.POLYMDEGRADSTAB.2006.03.022.
   523 (54) Virtanen, P.; Gommers, R.; Oliphant, T. E.; Haberland, M.; Reddy, T.; Cournapeau, D.;
- Burovski, E.; Peterson, P.; Weckesser, W.; Bright, J.; van der Walt, S. J.; Brett, M.; 524 525 Wilson, J.; Millman, K. J.; Mayorov, N.; Nelson, A. R. J.; Jones, E.; Kern, R.; Larson, E.; 526 Carey, C. J.; Polat, İ.; Feng, Y.; Moore, E. W.; VanderPlas, J.; Laxalde, D.; Perktold, J.; 527 Cimrman, R.; Henriksen, I.; Quintero, E. A.; Harris, C. R.; Archibald, A. M.; Ribeiro, A. 528 H.; Pedregosa, F.; van Mulbregt, P.; Vijaykumar, A.; Bardelli, A. Pietro; Rothberg, A.; 529 Hilboll, A.; Kloeckner, A.; Scopatz, A.; Lee, A.; Rokem, A.; Woods, C. N.; Fulton, C.; 530 Masson, C.; Häggström, C.; Fitzgerald, C.; Nicholson, D. A.; Hagen, D. R.; Pasechnik, D. 531 V.; Olivetti, E.; Martin, E.; Wieser, E.; Silva, F.; Lenders, F.; Wilhelm, F.; Young, G.; 532 Price, G. A.; Ingold, G. L.; Allen, G. E.; Lee, G. R.; Audren, H.; Probst, I.; Dietrich, J. P.; 533 Silterra, J.; Webber, J. T.; Slavič, J.; Nothman, J.; Buchner, J.; Kulick, J.; Schönberger, J. 534 L.; de Miranda Cardoso, J. V.; Reimer, J.; Harrington, J.; Rodríguez, J. L. C.; Nunez-535 Iglesias, J.; Kuczynski, J.; Tritz, K.; Thoma, M.; Newville, M.; Kümmerer, M.; 536 Bolingbroke, M.; Tartre, M.; Pak, M.; Smith, N. J.; Nowaczyk, N.; Shebanov, N.; Pavlyk, 537 O.; Brodtkorb, P. A.; Lee, P.; McGibbon, R. T.; Feldbauer, R.; Lewis, S.; Tygier, S.; 538 Sievert, S.; Vigna, S.; Peterson, S.; More, S.; Pudlik, T.; Oshima, T.; Pingel, T. J.; 539 Robitaille, T. P.; Spura, T.; Jones, T. R.; Cera, T.; Leslie, T.; Zito, T.; Krauss, T.; 540 Upadhyay, U.; Halchenko, Y. O.; Vázquez-Baeza, Y. SciPy 1.0: Fundamental Algorithms 541 for Scientific Computing in Python. Nature Methods 2020 17:3 2020, 17 (3), 261–272.

https://doi.org/10.1038/s41592-019-0686-2.

- 543 (55) Noda, I.; Ozaki, Y. Two-Dimensional Correlation Spectroscopy Applications in
- Vibrational and Optical Spectroscopy. Two-Dimensional Correlation Spectroscopy -
- 545 Applications in Vibrational and Optical Spectroscopy 2005.
- 546 https://doi.org/10.1002/0470012404.
- 547 (56) Sari, A.; Alkan, C.; Biçer, A.; Karaipekli, A. Synthesis and Thermal Energy Storage
- 548 Characteristics of Polystyrene-Graft-Palmitic Acid Copolymers as Solid-Solid Phase
- Change Materials. Solar Energy Materials and Solar Cells 2011, 95 (12), 3195–3201.
- 550 https://doi.org/10.1016/J.SOLMAT.2011.07.003.
- 551 (57) Alsharaeh, E. H.; Othman, A. A. Microwave Irradiation Synthesis and Characterization of
- RGO-AgNPs/Polystyrene Nanocomposites. Polym Compos 2014, 35 (12), 2318–2323.
- 553 https://doi.org/10.1002/PC.22896.
- 554 (58) Berruezo, M.; Ludueñ, L. N.; Rodriguez, E.; Alvarez, V. A. Preparation and
- Characterization of Polystyrene/Starch Blends for Packaging Applications. *Journal of*
- 556 Plastic Film & Sheeting **2014**, 30 (2), 141–161.
- 557 https://doi.org/10.1177/8756087913504581.
- 558 (59) Hu, H.; Wang, X.; Wang, J.; Wan, L.; Liu, F.; Zheng, H.; Chen, R.; Xu, C. Preparation
- and Properties of Graphene Nanosheets-Polystyrene Nanocomposites via in Situ
- 560 Emulsion Polymerization. *Chem Phys Lett* **2010**, 484 (4–6), 247–253.
- 561 https://doi.org/10.1016/J.CPLETT.2009.11.024.

- 562 (60) Topala, I.; Rusu, G.; Asandulesa, M.; Totolin, M.; Pohoata, V.; Dumitrascu, N.
- Functionalization of AFM Tips by Atmospheric Pressure Plasma Polymerization.
- 564 (61) Wang, C.; Qi, X.; Wang, Y.; Tian, Y. Room-Temperature Direct Heterogeneous Bonding
- of Glass and Polystyrene Substrates. J. Electrochem. Soc 2018.
- 566 https://doi.org/10.1149/2.0151808jes.
- 567 (62) Lucki, J.; Ranby; Ranby, B.; Lucki, J. B. New Aspects of Photodegradation and
- Photooxidation of Polystyrene. Pure and Applied Chemistry 1980, 52 (2), 295–303.
- 569 https://doi.org/10.1351/pac198052020295.
- 570 (63) Lucki, J.; Rånby, B. Photo-Oxidation of Polystyrene—Part 2: Formation of Carbonyl
- Groups in Photo-Oxidised Polystyrene. *Polym Degrad Stab* **1979**, 1 (3), 165–179.
- 572 https://doi.org/10.1016/0141-3910(79)90014-4.
- 573 (64) León-Bermúdez, A.-Y.; Salazar, R. SYNTHESIS AND CHARACTERIZATION OF THE
- 574 POLYSTYRENE-ASPHALTENE GRAFT COPOLYMER BY FT-IR
- 575 SPECTROSCOPY. Tecnología y Futuro 2008, 3.
- 576 (65) Nowakowska, M.; Kowal, J.; Waligora, B. Photo-Oxidation of Polystyrene Film: 2.
- Photo-Oxidation of Polystyrene Film with Light Absorbed by the Polystyrene-Oxygen
- 578 Complex. Polymer (Guildf) 1978, 19 (11), 1317–1319. https://doi.org/10.1016/0032-
- 579 3861(78)90314-2.

- 580 (66) Lucki, J.; Rånby, B. Photo-Oxidation of Polystyrene-Part 3. Photo-Oxidation of 2-Phenyl
- Butane as Model Compound for Polystyrene. *Polym Degrad Stab* **1979**, *1* (4), 251–276.
- 582 https://doi.org/10.1016/0141-3910(79)90001-6.
- 583 (67) Jaleh, B.; Madad, M. S.; Farshchi Tabrizi, M.; Habibi, S.; Golbedaghi, R.; Keymanesh, M.
- R. Iranian Chemical Society UV-Degradation Effect on Optical and Surface Properties of
- Polystyrene-TiO 2 Nanocomposite Film. *JOURNAL OF THE* **2011**, *8*, 161–168.
- 586 (68) Jang, B. N.; Wilkie, C. A. The Thermal Degradation of Polystyrene Nanocomposite.
- 587 Polymer (Guildf) **2005**, 46 (9), 2933–2942.
- 588 https://doi.org/10.1016/J.POLYMER.2005.01.098.
- 589 (69) Mailhot, B.; Gardette, J. L. Polystyrene Photooxidation. 2. A Pseudo Wavelength Effect.
- 590 *Macromolecules* **1992**, 25 (16), 4127–4133.
- 591 https://doi.org/10.1021/MA00042A013/ASSET/MA00042A013.FP.PNG V03.
- 592 (70) Kovačević, V.; Bravar, M.; Lorvić, L.; Šegudović, N.; Hace, D. GPC and Structural
- Analysis of Polystyrene Degradation. *Polymer Photochemistry* **1984**, 4 (6), 459–472.
- 594 https://doi.org/10.1016/0144-2880(84)90056-3.
- 595 (71) Liang, C. Y.; Krimm, S. Infrared Spectra of High Polymers. VI. Polystyrene. Journal of
- 596 *Polymer Science* **1958**, 27 (115), 241–254.
- 597 https://doi.org/10.1002/POL.1958.1202711520.

- 598 (72) Tian, L.; Ma, Y.; Ji, R. Quantification of Polystyrene Plastics Degradation Using 14C
- Isotope Tracer Technique. Methods Enzymol 2021, 648, 121–136.
- 600 https://doi.org/10.1016/BS.MIE.2020.12.014.
- 601 (73) Ward, C. P.; Armstrong, C. J.; Walsh, A. N.; Jackson, J. H.; Reddy, C. M. Sunlight
- 602 Converts Polystyrene to Carbon Dioxide and Dissolved Organic Carbon. 2019.
- 603 https://doi.org/10.1021/acs.estlett.9b00532.
- 604 (74) Hernández, C. G.; González, R.; Soto, J. J.; Rosales, I. Photo-Oxidation of Polystyrene
- Film Irradiated with UV-B. Conference Proceedings of the Society for Experimental
- 606 Mechanics Series 2017, 2017-Janua, 295–299. https://doi.org/10.1007/978-3-319-28513-
- 607 9 41/COVER.
- 608 (75) Shang, J.; Chai, M.; Zhu, Y. Solid-Phase Photocatalytic Degradation of Polystyrene
- Plastic with TiO2 as Photocatalyst. J Solid State Chem 2003, 174 (1), 104–110.
- 610 https://doi.org/10.1016/S0022-4596(03)00183-X.
- (76) Rabek, J. F.; Ranby, B. Studies on the Photooxidation Mechanism of Polymers. I. Photolysis and
- Photooxidation of Polystyrene. Journal of Polymer Science: Polymer Chemistry Edition 1974,
- 613 12 (2), 273–294. https://doi.org/10.1002/POL.1974.170120203.
- 614 (77) Wang, X.; Zheng, H.; Zhao, J.; Luo, X.; Wang, Z.; Xing, B. Photodegradation Elevated
- the Toxicity of Polystyrene Microplastics to Grouper (Epinephelus Moara) through
- Disrupting Hepatic Lipid Homeostasis. *Environ Sci Technol* **2020**, *54* (10), 6202–6212.

- 617 https://doi.org/10.1021/ACS.EST.9B07016/ASSET/IMAGES/LARGE/ES9B07016 0005.
- JPEG.
- 619 (78) Wu, X.; Chen, X.; Jiang, R.; You, J.; Ouyang, G. New Insights into the Photo-Degraded
- Polystyrene Microplastic: Effect on the Release of Volatile Organic Compounds. J
- 621 *Hazard Mater* **2022**, *431*, 128523. https://doi.org/10.1016/J.JHAZMAT.2022.128523.
- 622 (79) Achhammer, B. G.; Reiney, M. J.; Wall, L. A.; Reinhart, F. W. Study of Degradation of
- Polystyrene by Means of Mass Spectrometry. Journal of Polymer Science 1952, 8 (5),
- 624 555–571. https://doi.org/10.1002/POL.1952.120080513.
- 625 (80) Gardette, J. L.; Mailhot, B.; Lemaire, J. Photooxidation Mechanisms of Styrenic
- Polymers. Polym Degrad Stab 1995, 48 (3), 457–470. https://doi.org/10.1016/0141-
- 627 3910(95)00113-Z.
- 628 (81) Ranby, B.; Lucki, J. New Aspects of Photodegradation and Photo-Oxidation of
- 629 Polystyrene. Pure and Applied Chemistry **1980**, 52 (2), 295–303.
- https://doi.org/10.1351/PAC198052020295/MACHINEREADABLECITATION/RIS.
- 631 (82) Chamas, A.; Moon, H.; Zheng, J.; Qiu, Y.; Tabassum, T.; Jang, J. H.; Abu-Omar, M.;
- Scott, S. L.; Suh, S. Degradation Rates of Plastics in the Environment. ACS Sustain Chem
- Eng **2020**, 8 (9), 3494–3511. https://doi.org/10.1021/acssuschemeng.9b06635.

- 634 (83) Liu, P.; Qian, L.; Wang, H.; Zhan, X.; Lu, K.; Gu, C.; Gao, S. New Insights into the Aging
- Behavior of Microplastics Accelerated by Advanced Oxidation Processes. 2019.
- https://doi.org/10.1021/acs.est.9b00493.
- 637 (84) Ferrer-Ugalde, A.; Juárez-Pérez, E. J.; Teixidor, F.; Viñas, C.; Sillanpää, R.; Pérez-
- Inestrosa, E.; Núñez, R. Synthesis and Characterization of New Fluorescent Styrene-
- 639 Containing Carborane Derivatives: The Singular Quenching Role of a Phenyl Substituent.
- 640 Chemistry A European Journal **2012**, 18 (2), 544–553.
- 641 https://doi.org/10.1002/CHEM.201101881.
- 642 (85) Lizotte, J. R.; Long, T. E. Stable Free-Radical Polymerization of Styrene in Combination
- with 2-Vinylnaphthalene Initiation. *Macromol Chem Phys* **2003**, 204 (4), 570–576.
- https://doi.org/10.1002/MACP.200390020.
- 645 (86) Lewis, F. D.; Wagner-Brennan, J. M.; Miller, A. M. Formation and Behavior of
- Intramolecular N-(Styrylalkyl)Aniline Exciplexes. https://doi.org/10.1139/v98-229 2011,
- 647 77 (5–6), 595–604. https://doi.org/10.1139/V98-229.
- 648 (87) Gardette, J. L.; Mailhot, B.; Lemaire, J. Photooxidation Mechanisms of Styrenic
- Polymers. Polym Degrad Stab 1995, 48 (3), 457–470. https://doi.org/10.1016/0141-
- 650 3910(95)00113-Z.
- 651 (88) MacCallum, J. R.; Ramsay, D. A. The Photo-Oxidation of Styrene-Type Copolymers-I.
- 652 Eur Polym J 1977, 13 (12), 945–948. https://doi.org/10.1016/0014-3057(77)90163-X.

- 653 (89) Rabek, Jan. F. *Polymer Photodegradation: Mechanisms and Experimental Methods*;
  654 Springer Netherlands, 1995. https://doi.org/10.1007/978-94-011-1274-1.
- 655 (90) Rånby, B. Photodegradation and Photo-Oxidation of Synthetic Polymers. *J Anal Appl Pyrolysis* **1989**, *15* (C), 237–247. https://doi.org/10.1016/0165-2370(89)85037-5.
- (91) Tarek, A. R.; Rasco, B. A.; Sablani, S. S. Ultraviolet-C Light Inactivation Kinetics of E.
   Coli on Bologna Beef Packaged in Plastic Films. https://doi.org/10.1007/s11947-015 1487-y.
- Turton, T. J.; White, J. R. Effect of Stabilizer and Pigment on Photo-Degradation Depth Profiles in Polypropylene. *Polym Degrad Stab* **2001**, 74 (3), 559–568. https://doi.org/10.1016/S0141-3910(01)00193-8.
- (93) Nagai, N.; Matsunobe, T.; Imai, T. Infrared Analysis of Depth Profiles in UV Photochemical Degradation of Polymers. *Polym Degrad Stab* 2005, 88 (2), 224–233.
   https://doi.org/10.1016/J.POLYMDEGRADSTAB.2004.11.001.